Contact Stability Analysis of Magnetically-Actuated Robotic Catheter Under Surface Motion

Ran Hao, Tipakorn Greigarn, M. Cenk Çavuşoğlu

Abstract— **Contact force quality is one of the most critical factors for safe and effective lesion formation during cardiac ablation. The contact force and contact stability plays important roles in determining the lesion size and creating a gap-free lesion. In this paper, the contact stability of a novel magnetic resonance imaging (MRI)-actuated robotic catheter under tissue surface motion is studied. The robotic catheter is modeled using a pseudo-rigid-body model, and the contact model under surface constraint is provided. Two contact force control schemes to improve the contact stability of the catheter under heart surface motions are proposed and their performance are evaluated in simulation.**

I. Introduction

Radiofrequency catheter ablation is the cornerstone of atrial fibrillation treatment [1]. During radiofrequency ablation, the catheter needs to maintain steady contact with the substrate tissue with appropriate contact force to create a transmural scar, in order to create a gap-free lesion. This paper focuses on the development of methods for achieving robust contact stability of the novel magnetic resonance imaging (MRI)-actuated robotic intravascular cardiac catheter system (presented in [2], [3]) while in contact with cardiac tissue under cardiac motions. This type of robotic catheter operates inside the bore of an MRI scanner and is magnetically actuated by a set of electromagnetic coils embedded on the catheter, in interaction with the MRI scanner's magnetic field, where the actuation of the catheter is controlled by the currents passing through the coils [2], [4], [5].

The disturbance caused by heart surface motions can lead to unpredictable lesion formation during ablation; as such, maintaining stable contact while being subjected to the beating heart motions is critical. Maintaining the contact force to remain inside the friction cone during the cardiac motion will reduce the possibility of sliding and positional errors, while sustaining an adequate contact force will ensure the formation of a transmural lesion. In this paper, we investigate the contact stability of the MRI-actuated robotic catheter during cardiac motion. A contact model for the Pseudo-Rigid-Body model of the catheter is introduced. The contact force actuation Jacobian that approximates the relationship between the change of the contact force and the change of the actuation currents is then formulated. A quasi-static contact force control method based on the proposed contact model is then presented. Given an instantaneous tissue surface, the proposed contact force control method is applied to drive the contact force inside the friction cone and provide a safe normal force for a target contact point on the tissue surface. Two dynamic contact force control schemes are then proposed to improve the contact stability under heart surface motions. The first method is a least square based contact force control scheme, which minimizes the contact force residuals over a horizon of estimated heart beat positions, relying on the quasi-periodic nature of the cardiac motion. The second method is an online actuation current update scheme, where the actuation currents calculated by the quasi-static contact force control method are updated at the servo control rate during the heart surface motions. Finally, the simulation-based validations of the two contact force control schemes are presented. The contact stability and the robustness of the proposed contact force control schemes are discussed and evaluated.

The rest of this paper is organized as follows. Related work is presented in Section II. The pseudo-rigid-body model of the robot under surface constraint is reviewed and presented in Section III. The quasi-static contact force control algorithm and dynamic contact force control schemes are provided in Section IV. The contact stability analysis and simulation-based validations of the contact force control schemes are presented in Section V. Conclusions are presented in Section VI.

II. Related Work

The role of catheter-tissue contact in catheter interventions is critical to the success of radiofrequency ablation procedures [6]. A number of factors have been shown to have great impact on the lesion formation during the ablation, including ablation circuit impedance [7], tissue architecture, myocardial blood flow [8], and contact stability. Adequate contact force becomes the key determinant to transfer the heat energy to the target tissue surface and an effective lesion formation [8], [9]. Insufficient contact force can lead to failure of tissue heating despite enough power [7]; Respiration is the main cause of relative motion of cardiac structures [10], [11], which can result in positional errors and inadequate or excessive contact force during the atrial ablation. Limiting force variations is an effective way of minimizing the ablation complications cause by the respiration [11].

The relationship between the contact force and the lesion formation during atrial fibrillation ablation has been widely

This work was supported in part by the National Science Foundation under grants CISE IIS-1524363, CISE IIS-1563805, ENG IIP-1700839, and National Institutes of Health under grant R01 EB018108.

RH and MCC are with the Department of Electrical, Computer, and Systems Engineering, Case Western Reserve University, Cleveland, OH. TG was with the Department of Electrical Engineering and Computer Science, Case Western Reserve University, Cleveland, OH. They can be reached via email at {rxh349,txg92,mcc14}@case.edu respectively.

studied. Force-sensing radiofrequency ablation catheter plays an important role in measuring the contact force [1], [6], [7], [12]. In [8], contact force is measured and analyzed during pulmonary vein isolation using a contact force sensor. This study suggests that the contact force for achieving clinical efficacy in ablation should be >10g (0.1N), and is best controlled with an average contact force >20g (0.2N). Wakili et al. [13] show that all patients treated with contact force <10g experienced arrhythmia recurrence. Andrade et al. [14] also show that contact force <10g is associated with higher rate of arrhythmia recurrence (100%) compared to contact force >20g (20%). Thiagalingam et al. [15] show the "moderate" catheter contact force, which is around 20g, can improve the possibility of creating reasonable lesion size. High power ablation and excessive contact force increases the risk of popping. In general, contact force >10g is required to guarantee a successful ablation. A desired contact force of 20g is suggested by [15] and [16]. In this study, we investigate the ability of the MRI-actuated robotic catheter to maintain the contact force in this narrow therapeutic range during the heart beat cycle [11], where we limit the desired range to 10g$\sim$25g (0.1N$\sim$0.25N).

Maintaining stable contact with the tissue surface during cardiac motion is essential for providing safe and reliable cardiac ablation procedures. Saliba et al. [17] compare the ablation results between the remote controlled robotic catheter system and manual ablation catheters. The experiments suggest that the efficacy of the robotic catheter system is similar to the conventional catheter systems. Di et al. [18] also show that using a remote robotic manipulation system can improve the efficacy and safety of ablation procedures. An image guided active robotic catheter is proposed in [19], where a closed-loop PID controller is used to regulate the tip position and force with additional sensors. Yuen et al. [20] present a design for a catheter tip force sensor and propose a feed-forward controller for contact force control. Kesner et al. [21] propose a robotic catheter system with 3D ultrasound image guidance and force control to keep a constant contact force against the tissue motion. Yip et al. [22] develop an adaptive Jacobian estimation method for closed-loop position-force control of a catheter under heart motion disturbances.

In this paper, we present the analysis of the contact stability of the MRI-actuated robotic catheter under cardiac tissue motions. Unlike the above studies, the contact force control schemes proposed in this paper are formulated without using additional force sensors, and the contact force control algorithms are proposed based on the calculation of the contact force actuation Jacobian.

III. Pseudo-Rigid-Body Model of the Catheter

In the Pseudo-Rigid-Body (PRB) model, the catheter is modeled as a series of pseudo-rigid links connected by elastic joints (Fig. 1) [23]–[26]. Each joint is modeled as a spherical joint which is parametrized by rotation angles in a set of axis angle representations $\theta_i = [\theta_{i1}, \theta_{i2}, \theta_{i3}]^T$ [27], which implies

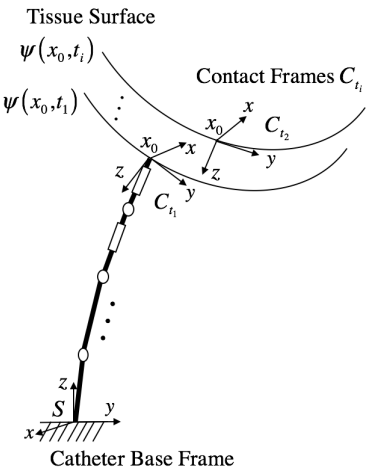

Fig. 1. The pseudo-rigid-body model of the robotic catheter with two sets of tri-axial actuation coils subject to the surface contact constraint. The contact frame C is chosen such that its origin is located at the contact point of the catheter and the z-axis is the outward normal of the tissue surface. x_0 denotes the contact point position in surface frame, which remains static during heart surface motion. The spatial frame S is given as shown.

non-ordered rotations. The twist of the i-th joint is given as

$$\xi_i(\theta_i) = \begin{bmatrix} -\theta_i \times q_i \\ \theta_i \end{bmatrix}, \tag{1}$$

where q_i is the initial position of the i-th joint in spatial frame. The shape of the catheter under the $n+1$-link PRB model can then be described by the joint angle vector $\theta = [\theta_1^T, \theta_2^T, \ldots, \theta_n^T]^T \in \mathbf{C} \subset \mathbb{R}^{3n}$, where $\mathbf{C}$ denotes the configuration space of the catheter robot [27]. And the forward kinematics of the catheter is given as [28]:

$$g_{st}(\theta) \;=\; e^{\hat{\xi}_1\theta_1} e^{\hat{\xi}_2\theta_2} \ldots e^{\hat{\xi}_n\theta_n} g_{st}(0), \tag{2}$$

where S is the spatial frame, and T is catheter tip frame.

The currents $u = [u_1, .., u_i, .., u_M]^T$ applied to the actuation coils embedded on the catheter result in magnetic moments $n_i A_i u_i$ on the coils, where n_i and A_i are respectively the number of turns and the area vector (in body frame) of the i-th coil, $i = 1, .., M$, and M is the number of actuator coils. The resulting Lorentz forces generated on the coils by the static magnetic field of the MRI scanner are given by $(n_i A_i u_i)^\wedge B_i = -B_i^\wedge (n_i A_i) u_i$, where B_i is the static magnetic field of the MRI scanner in the body frame of the coil i, and $^\wedge$ is the cross product operator.

These actuation moments can then be mapped to the joint torques $\tau(\theta, u) \in \mathbb{R}^{3n}$ as [27]:

$$\tau(\theta, u) = \sum_i^M {J_{su_i}^b}^T \begin{bmatrix} 0 \\ B_i^\wedge (n_i A_i) \end{bmatrix} u_i = A(\theta) u. \tag{3}$$

Here, $J_{su_i}^b$ is the body Jacobian corresponding to coil i, and

$$A(\theta) = \begin{bmatrix} \ldots & {J_{su_i}^b}^T \begin{bmatrix} 0 \\ B_i^\wedge (n_i A_i) \end{bmatrix} & \ldots \end{bmatrix}, \tag{4}$$

$i = 1, .., M$. $\tau(\theta, u)$ will be denoted as τ_u in the rest of the paper for convenience.

A. Contact Model

Coulomb friction is employed to model the friction forces between the catheter tip and the surface. In Coulomb friction model, the friction cone is defined as:

$$FC = \{f_c \in \mathbb{R}^3 \ : \ \sqrt{{\lambda_{f1}}^2 + {\lambda_{f2}}^2} \leq \mu_s \lambda_c\}, \tag{5}$$

where f_c denotes the contact force, μ_s denotes the Coulomb friction coefficient, and λ_c and λ_{fi} respectively denote the normal and the two tangential components of the contact force. The set of contact forces which cause no slippage between the tip and the surface must lie in the friction cone. Suppose the contact between catheter and the surface is non-conforming, the origin of the contact frame is located at the contact point, and its z-axis is in the outward surface normal direction. Then the contact force would be in the form by $f_c = [\lambda_{f1}, \lambda_{f2}, \lambda_c]$. The associated contact Jacobian $J_C \in \mathbb{R}^{3\times 3n}$ relating contact forces to joint torques [29] is given by:

$$J_C = \mathbf{B}_c^T \mathrm{Ad}_{g_{sc}^{-1}} J_{st}^s, \tag{6}$$

$$\mathbf{B}_c = \begin{bmatrix} 1, & 0, & 0 \\ 0, & 1, & 0 \\ 0, & 0, & 1 \\ 0, & 0, & 0 \\ 0, & 0, & 0 \\ 0, & 0, & 0 \end{bmatrix}, \tag{7}$$

$$\mathrm{Ad}_{g_{sc}^{-1}} = \begin{bmatrix} R_{sc}^T, & -R_{sc}^T \hat{p_{sc}} \\ 0, & R_{sc}^T \end{bmatrix}, \tag{8}$$

where J_{st}^s denotes the spatial manipulator Jacobian of the catheter. g_{sc} denotes the transformation from the contact frame to the spatial frame, and, R_{sc} and p_{sc} are respectively the rotational and translational components of the contact frame to spatial frame transformation.

The quasi-static equilibrium[1] equation of the catheter describing the relationship between the catheter shape and the actuation currents under the tip contact position constraint is given by:

$$N(\theta) \ + \ K\theta \ - \ J_C^T f_c - \ \tau_u = 0, \tag{9}$$

where K is the stiffness coefficient matrix, and N is the gravitational effect term. The contact force is then calculated as:

$$f_c = {J_C^T}^{\dagger}(N(\theta) + \ K\theta - \ \tau_u), \tag{10}$$

where ${J_C^T}^{\dagger}$ is the left pseudo-inverse of J_C^T with ${J_C^T}^{\dagger} = (J_C J_C^T)^{-1} J_C$.

The contact ratio σ_μ between friction force and normal force is defined as:

$$\sigma_\mu(\theta, u) = \frac{\|\lambda_f\|}{\lambda_c}, \tag{11}$$

where $\sigma_\mu \in \mathbb{R}$. The catheter remains on the target contact point if the contact force is inside the friction cone FC, or equivalently, $0 \leq \sigma_\mu \leq \mu_s$ where μ_s is the friction coefficient between the catheter tip and the tissue surface.

[1]Since the catheter moves with low velocity and acceleration during catheter ablation, the inertial and Coriolis forces are negligible, and therefore can be neglected.

B. Contact Force Actuation Jacobian

In this section, contact force-actuation Jacobian is derived to approximate the relationship between the changes in contact forces and the changes in actuation currents.

Substituting (3) into the quasi-static equation (9) as

$$J_C^T f_c = N(\theta) + K\theta - A(\theta)u. \tag{12}$$

At a given joint configuration θ_0, $A(\theta)$ and $N(\theta)$ can then be approximated at θ_0 using Taylor's theorem as $A(\theta) \approx A(\theta_0) + A'(\theta_0)\Delta\theta$ and $N(\theta) \approx N(\theta_0) + N'(\theta_0)\Delta\theta$, where $A'(\theta_0) = \partial A/\partial\theta|_{\theta=\theta_0}$[2] and $N'(\theta_0) = \partial N/\partial\theta|_{\theta=\theta_0}$. Then (12) can be linearized as

$$J_C^T f_c \approx (N(\theta_0) + N'(\theta_0)\Delta\theta) + K\theta_0 - (A(\theta_0) + A'(\theta_0)\Delta\theta)u. \tag{13}$$

Since the joint displacement $\Delta\theta$ is small based on the quasi-static assumption, (13) can be approximated as

$$J_C^T f_c \approx N(\theta_0) + K\theta_0 - A(\theta_0)u. \tag{14}$$

The contact force-actuation Jacobian J_{cu} at joint configuration θ_0 is then calculated as $J_{cu} = df_c/du \approx -{J_c^T}^{\dagger} A(\theta_0)$.

IV. Contact Force Control Under Surface Motion

Consider a given target catheter tip position on the tissue surface. This target position is assumed to be static in the surface frame, as shown in Fig. 1. The goal of the contact force control is to improve the stability of the contact between the catheter and the tissue surface under heart surface motion, namely, maintaining static catheter tip positioning at the desired location on the tissue surface with adequate normal contact force, despite cardiac motion.

In this section, first a quasi-static contact force control algorithm which computes a set of actuation currents for a desired normal contact force and target tip position for a given instantaneous surface configuration is introduced (Algorithm 1). Following this, two dynamic contact force schemes, which aim to maintain stable contact between the catheter and the tissue surface under cardiac motion.

In order to facilitate the subsequent presentation, let $\Psi(x,t)$ be a parametrization of the tissue surface, $x = x_0$ be the location of the desired contact point in the local tissue coordinates, and t denote the time.

A. Quasi-Static Contact Force Control Algorithm

The proposed quasi-static contact force control algorithm is presented in Algorithm 1. The algorithm computes the actuation currents for a desired normal contact force and target tip position on a given instantaneous surface configuration, neglecting the heart surface motion (hence the name quasi-static).

The algorithm assumes that the catheter tip is initially in contact with the target point on the tissue surface. The

[2]Note that $A'(\theta_0)$ is a tensor and $A'(\theta_0) \in R^{3n\times M\times 3n}$

Algorithm 1: Quasi-Static Contact Force Control With Tip Position Constraint for Robotic Catheter

Input : u^0, f_{cn}^d, $\Psi(x_0)$

1 t $\leftarrow 0$
2 **while** $|f_{cn}^d - f_{cn}^t| > \varepsilon$ **do**
3 $\quad \theta^t \leftarrow$ constrained_equilibrium$(u^t, \Psi(x_0))$
4 $\quad {f_c}^t \leftarrow$ compute_contact_force(θ^t, u^t)
5 $\quad k_n^t \leftarrow \alpha(f_{cn}^d - f_{cn}^t)$
6 $\quad d{f_c}^t \leftarrow (-f_{cx}^t, -f_{cy}^t, k_n^t)$
7 $\quad J_{cu} \leftarrow -{J_C^T}^{\dagger} A(\theta^t)$
8 $\quad du \leftarrow J_{cu}^{\dagger} d{f_c}^t$
9 $\quad u^{t+1} \leftarrow u^t + du$
10 $\quad$ t $\leftarrow$ t + 1
11 **end**

Output: u^t

initial actuation current u^0, the desired normal contact force f_{cn}^d, and the spatial coordinates of the contact point on the tissue surface $\Psi(x_0)$ are given as inputs. In this algorithm, the contact force is controlled for a given instantaneous configuration of the surface; thus, the time parametrization t in $\Psi(x_0,t)$ is excluded. In Line 3, the quasi-static equilibrium configuration of the catheter is computed for the given input currents and the tissue surface contact point using a potential energy minimization based algorithm [28], [30]. The contact force f_c is then updated given the updated joint angles and actuation currents. The change of the normal contact force k_n^t is calculated from the desired normal component of the contact force in Line 5, where α is the step size to adjust the updating speed. The incremental change of the contact force df_c is calculated in Line 6. A negative feedback is applied on the tangential forces to keep the contact force inside the friction cone during the contact control, while the normal component is driven towards the desired value. In line 7, the contact force actuation Jacobian J_{cu} is computed given current joint configurations. The incremental current update du is computed and applied respectively in Lines 8 and 9.

B. Dynamic Contact Force Control Algorithms

The goal of the dynamic contact force control algorithms is to select an actuation current set that would maintain stable contact between the catheter and the tissue surface under cardiac motion.

The first dynamic contact force control scheme proposed aims to identify a single actuation current set that would be constantly applied and would maintain a stable contact throughout the subsequent cardiac cycles. Selection of such a single actuation level would require an estimate of the future motion of the heart. There are a number of heart motion estimation schemes proposed in the literature (e.g., [31]–[36]), which take advantage of the quasi-periodic nature of the heart motion. In this study, a relatively simple estimation scheme, which uses the motion during the previous heart cycle as an estimate of the range of motions during subsequent cycles, is employed [37]. The algorithm then iteratively

Algorithm 2: Least Square Based Contact Force Control With Tip Position Constraint Under Surface Motion

Input : u^0, $\{\Psi(x_0,t_i),\ i = 1,..,m\}$

1 $j \leftarrow 0$
2 **repeat**
3 $\quad$ **for** *all i in heart beat cycle {1, 2, ..., m}* **do**
4 $\quad\quad \theta_i^t \leftarrow$ constrained_equilibrium$(u^t, \Psi(x_0,t_i))$
5 $\quad\quad J_i \leftarrow -{J_C^T}^{\dagger} A(\theta_i^t)$
6 $\quad\quad f_{ci} \leftarrow$ compute_contact_force(θ_i^t, u^t)
7 $\quad\quad$ **if** $f_{ci}^n > ub$ **then**
8 $\quad\quad\quad df_c^n \leftarrow -k_n$
9 $\quad\quad$ **end**
10 $\quad\quad$ **if** $f_{ci}^n < lb$ **then**
11 $\quad\quad\quad df_c^n \leftarrow k_n$
12 $\quad\quad$ **end**
13 $\quad\quad df_{ci} \leftarrow (-k_f f_{ci}^x, -k_f f_{ci}^y, df_{ci}^n)$
14 $\quad$ **end**
15 $\quad J \leftarrow [J_1^T, J_2^T, ..., J_m^T]^T$
16 $\quad df_c \leftarrow [df_{c1}^T, df_{c2}^T, ..., df_{cm}^T]^T$
17 $\quad du \leftarrow (J^T W_I J)^{-1} J^T W_I df_c$
18 $\quad u^{j+1} \leftarrow u^j + du$
19 $\quad$ j $\leftarrow$ j + 1
20 **until** *(*$j =$ IterationLimit*)* or *(*$\|du\| < \varepsilon$*)*;

Output: u^j

computes the actuation current value that best approximates the desired contact force vector over the estimated heart motion trajectory in a least squares sense.

The full least square based contact force control algorithm is given in Algorithm 2. The algorithm again assumes that the catheter tip is initially in contact with the target point on the tissue surface. The initial actuation current u^0, and the spatial coordinates of the predicted positions of the contact point on the tissue surface $\{\Psi(x_0,t_i), i = 1,..,m\}$ are given as inputs. The algorithm first collects the contact force actuation Jacobians and the calculated incremental changes of the contact forces for all of the tip positions throughout the estimated heart motion cycle. Specifically, for each tip position in the heart beat cycle i, the equilibrium joint angles θ_i under catheter tip position constraint are obtained in Line 4. Similar to Algorithm 1, the contact force actuation Jacobian is calculated and collected by J_i in Line 5. A negative feedback $-k_f$ is applied on the tangential forces to keep the contact force inside the friction cone during the contact control. The normal contact force during the ablation procedure is required to be maintained between the force limits $lb = 0.1N \leq f_{ci} \leq ub = 0.25N$. The normal component of the contact force is incrementally changed in steps of k_n towards the bounds as shown in Lines 7-12. The desired contact force update df_{ci} is then computed as Line 13. Lines 15-17 compute the actuation current update du as a weighted least squares problem, where W_I is the weight matrix. The actuation currents are then updated in Line 18.

The advantage of this control scheme is the regularization of the contact forces over the control horizon provided

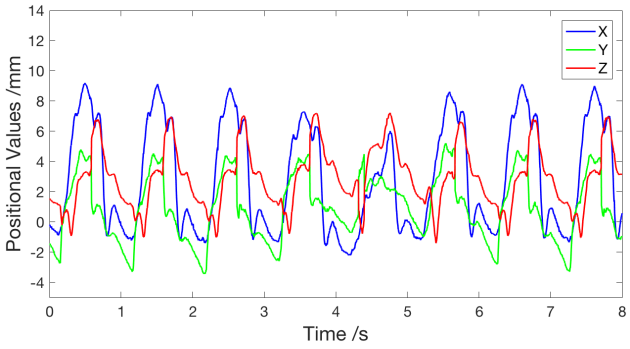

Fig. 2. The heart rate position data for 8s (2000 samples), corresponding to approximately 8 heart beat cycles, of the overall 60s long experimental heart motion dataset used in the simulation studies. The heart motion is quasi-periodic, as shown in the figure. In cycles 4 and 5, the heart motion experiences some irregularity.

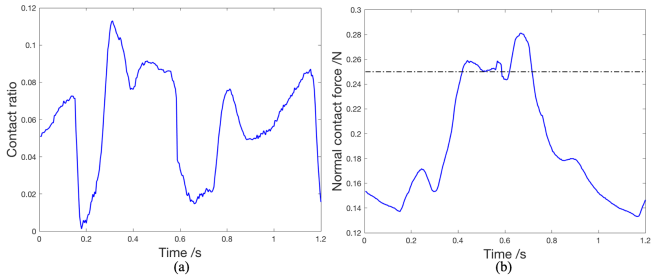

Fig. 3. (a) The contact ratio σ_μ over 1.2s of heart beat motion (300 samples) after actuation currents given by the quasi-static contact force control algorithm (Algorithm 1) are applied. (b) The normal contact force over the same 1.2s of heart motion after the quasi-static contact force control. The upper force limit of 0.25N is marked by dashed line.

by the least squares optimization. The weakness of the method comes from its reliance on an estimation of the future motions of the contact point. The further the actual trajectories of the contact point deviate from the predicted motion, the higher the risk for the actual contact forces to violate the prescribed contact force bounds or to loose contact stability.

In the second dynamic contact force control scheme proposed, the actuation currents are updated at the servo control rate with the quasi-static contact force control algorithm as proposed in Algorithm 1, using the current location of the contact point on the instantaneous tissue surface $\Psi(x_0,t)$ approximately as quasi-static.

V. Simulation-Based Validation Studies

In this section, the results of the simulation-based validation studies evaluating the performance of the proposed control algorithms are presented.

The parameters of catheter robot model used in this paper are based on the parameters identified in [38] of our MRI-actuated robotic catheter prototype. The mechanical model of the catheter has 5 pseudo-rigid links, each with 20mm length, for a total catheter length of 100 mm. For evaluation of the control performance, we have used in vivo heart motion data collected in our earlier studies [35]. Specifically, the data used is a 60s long recording of the motion of a point-of-interest on a free beating heart with uniform heart rate, sampled at a 250Hz sampling rate. (Fig. 2).

First, the quasi-static contact force control algorithm proposed in Algorithm 1 is validated. The results of this validation study also demonstrate the need for the proposed dynamic contact force control algorithms. Specifically, in this simulation study, the heart beat position at $t = 0.18$s is chosen for providing an initial configuration, where the contact force control in Algorithm 1 is performed with desired normal contact force $f_{cn}^d = 0.15N$ in order to compute the initial actuation currents u^0. Fig. 3 shows the resulting contact ratio and normal contact force for the first 1.2s heart motion after the actuation currents given by Algorithm 1 are applied to the catheter. As shown in Fig. 3 (b), the normal contact force at $t = 0.18$s is 0.15N, while the normal forces at heart beat positions from 0.44s-0.72s exceed 0.25N limit. In this example, the contact ratios for all 300 heart beat samples happen to be under $\mu_s = 0.2$, the coefficient of friction between the catheter and the atrial surface [3]; however, variations in heart motion may have easily lead to violation of this condition, since the actuation currents were determined without any consideration for heart motions.

For validation of the least square based dynamic contact force control scheme, the first 1.2s (300 samples) of the heart motion data is used as the prediction of the heart motion for the subsequent heart beats. The least squares optimization algorithm presented in Algorithm 2 is executed over these 300 sample points of the estimated target motion trajectory, with the update rates of normal and tangential force $k_n = 0.0007$, $k_f = 0.001$, respectively. The change of the contact ratios over the estimated motion trajectory during the iterations of the least squares computation is shown in Fig. 4 (a). The contact force before and after the least square based contact control over the estimated motion trajectory are presented in Fig. 4 (b). These results demonstrate the operation of the least-square based contact control, showing how these quantities progress over the iterations, bringing the quantities to within the desired limits. Specifically, as shown in Fig. 4, the least square based contact force control drives the contact force within 0.1N $\sim$ 0.25N, and the contact ratio to below 0.2, ensuring contact stability and safe contact forces for the estimated motion trajectory.

The robustness of the obtained actuation currents are then tested with the subsequent cycles of the heart motion. Specifically, the actuation currents calculated by the least squares based dynamic contact force control algorithm from the first heart beat (first 1.2s of data) are used for the subsequent 4 heart beat cycles, and the resulting contact ratios and normal contact forces are shown in Fig. 5. In Fig. 5 (a), the contact ratio for all the heart beat cycles are below 0.2. Due to the irregularity of the heart beat cycle 4 and 5, as indicated in Fig. 2, the normal contact force increased above 0.25N for some heart beat points during these 2 cycles. This is caused by the imperfect motion prediction, which assumes that the heart beat motions in subsequent cycles exactly repeat the first heart beat cycle.

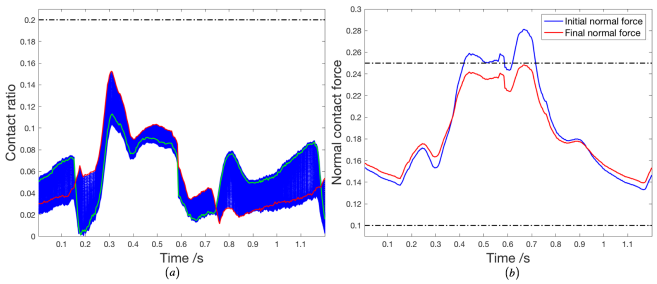

Fig. 4. (a) The change of the contact ratio over the estimated motion trajectory through 40 iterations of the least square optimization. The green curve marks the initial contact ratios, the blue curves mark the change of the contact ratios during the iterations, and the red curve marks the final contact ratios. The contact ratio limit of $\mu_s = 0.2$ is marked by the dashed line. (b) The initial normal contact force and the final contact force over the estimated motion trajectory. The upper and lower force limits are marked by the dashed lines.

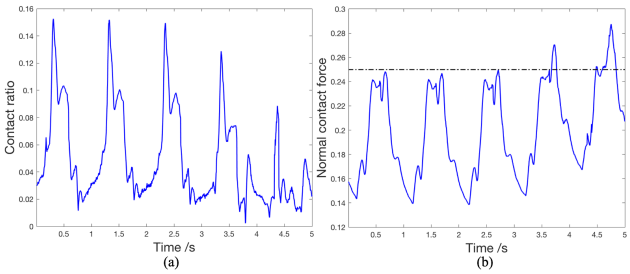

Fig. 5. (a) Contact ratio over the first 5 heart beat cycles (5.0s) after the least square based contact force control. (b) Normal contact forces over the first 5 heart beat cycles. The upper force limit of 0.25N is marked by dashed line.

Next, the second dynamic contact force control scheme where the the actuation currents are updated at the servo control rate is evaluated. In the simulation study, a servo control sampling period of 48ms, approximately matching the targeted servo control rate of 20Hz of the prototype catheter system [39], is used. Specifically, the quasi-static contact force control method in Algorithm 1 is performed at 48ms intervals using the instantaneous target position of the catheter. A desired normal contact force value of $f_{cn}^{d} = 0.15N$ is used in the algorithm. The actuation currents computed by the algorithm are then applied to the catheter for the 48ms sampling duration, until the next sample time, while the 'actual' contact forces and contact ratios are calculated at the full sampling rate of the underlying heart motion data. The calculated contact ratios and normal contact forces for 5 heart beat cycles are given in Fig. 6. As shown in Fig. 6, the contact ratio and normal contact force for the 5 heart beat cycles are within desired ranges.

VI. Conclusions

In this paper, the contact stability of the MRI-actuated robotic catheter under cardiac motions is studied. The catheter-tissue contact model based on Pseudo-Rigid-Body Model of the robotic catheter is formulated. A quasi-static contact force control algorithm is proposed to improve the contact stability given an instantaneous surface configuration. Two dynamic contact force control schemes are then presented. First, a least square based contact force control algorithm is proposed where a single actuation current set is calculated and applied over the full heart beat cycles. The second scheme, where the actuation currents calculated by the quasi-static contact force control algorithm are updated at servo control rate for the given heart surface motions, is also provided.

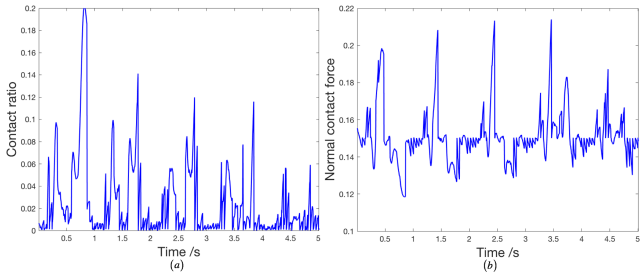

Fig. 6. (a) Contact ratio over the first 5 heart beat cycles. The actuation currents are updated every 12 heart beat points (48ms). (b) Normal contact forces over the first 5 heart beat cycles.

The simulation-based validations are presented for evaluating the performance of the two proposed contact force control schemes. For the given heart motion, the least square based dynamic control scheme is able to provide safe and stable contact force. Due to the limitation of the heart motion prediction method, the least square based control scheme is not robust to large irregularities of the heart motion. The validation results for the second dynamic contact force control scheme show that the contact force is driven within the safe ranges more robustly to irregularities in the heart motion, at the expense of the need for more frequent changes to the actuation current.

Even though the least square based contact force control failed at irregular motions, the robustness of the algorithm can be improved using better heart motion prediction methods. In our future work, we will incorporate more sophisticated heart motion prediction methods, such as, those presented in [31]–[36].

References

[1] A. Pedrote, J. Acosta, B. Jauregui-Garrido, M. Frutos-Lopez, and E. Arana-Rueda, "Paroxysmal atrial fibrillation ablation: Achieving permanent pulmonary vein isolation by point-by-point radiofrequency lesions," *World journal of cardiology*, vol. 9, no. 3, p. 230, 2017.

[2] T. Liu, N. L. Poirot, D. Franson, N. Seiberlich, M. A. Griswold, and M. C. Cavusoglu, "Modeling and validation of the three-dimensional deflection of an MRI-compatible magnetically actuated steerable catheter." *IEEE Trans. Biomed. Engineering*, vol. 63, no. 10, pp. 2142–2154, 2016.

[3] T. Liu, N. Lombard Poirot, T. Greigarn, and M. C. Çavuşoğlu, "Design of an MRI-guided magnetically-actuated steerable catheter," *ASME Journal of Medical Devices, Special Issue on Cardiovascular Device Development and Safety Assessment using Computational*

and/or Experimental Approaches, vol. 11, no. 2, p. 021004, 2017, cavusoglu:2015xg.

[4] T. Roberts, W. Hassenzahl, S. Hetts, and R. Arenson, "Remote control of catheter tip deflection: an opportunity for interventional MRI," *Magnetic Resonance in Medicine: An Official Journal of the International Society for Magnetic Resonance in Medicine*, vol. 48, no. 6, pp. 1091–1095, 2002.

[5] N. Gudino, J. Heilman, J. Derakhshan, J. Sunshine, J. Duerk, and M. Griswold, "Control of intravascular catheters using an array of active steering coils," *Medical Physics*, vol. 38, no. 7, pp. 4215–4224, 2011.

[6] N. Ariyarathna, S. Kumar, S. P. Thomas, W. G. Stevenson, and G. F. Michaud, "Role of contact force sensing in catheter ablation of cardiac arrhythmias: evolution or history repeating itself?" *JACC: Clinical Electrophysiology*, vol. 4, no. 6, pp. 707–723, 2018.

[7] H. Makimoto, T. Lin, A. Rillig, A. Metzner, P. Wohlmuth, A. Arya, M. Antz, S. Mathew, S. Deiss, E. Wissner *et al.*, "In vivo contact force analysis and correlation with tissue impedance during left atrial mapping and catheter ablation of atrial fibrillation," *Circulation: Arrhythmia and Electrophysiology*, vol. 7, no. 1, pp. 46–54, 2014.

[8] V. Y. Reddy, D. Shah, J. Kautzner, B. Schmidt, N. Saoudi, C. Herrera, P. Jaïs, G. Hindricks, P. Peichl, A. Yulzari *et al.*, "The relationship between contact force and clinical outcome during radiofrequency catheter ablation of atrial fibrillation in the toccata study," *Heart rhythm*, vol. 9, no. 11, pp. 1789–1795, 2012.

[9] L. Di Biase, A. Natale, C. Barrett, C. Tan, C. S. Elayi, C. K. Ching, P. Wang, A. AL-AHMAD, M. Arruda, J. D. Burkhardt *et al.*, "Relationship between catheter forces, lesion characteristics,popping, and char formation: experience with robotic navigation system," *Journal of cardiovascular electrophysiology*, vol. 20, no. 4, pp. 436–440, 2009.

[10] H. U. Klemm, D. Steven, C. Johnsen, R. Ventura, T. Rostock, B. Lutomsky, T. Risius, T. Meinertz, and S. Willems, "Catheter motion during atrial ablation due to the beating heart and respiration: Impact on accuracy and spatial referencing in three-dimensional mapping," *Heart Rhythm*, vol. 4, no. 5, pp. 587–592, 2007.

[11] P. A. Friedman, "Hitting a moving target: Catheter ablation and respiration," *Heart rhythm*, vol. 9, no. 7, pp. 1048–1049, 2012.

[12] K.-H. Kuck, V. Y. Reddy, B. Schmidt, A. Natale, P. Neuzil, N. Saoudi, J. Kautzner, C. Herrera, G. Hindricks, P. Jaïs *et al.*, "A novel radiofrequency ablation catheter using contact force sensing: Toccata study," *Heart rhythm*, vol. 9, no. 1, pp. 18–23, 2012.

[13] R. Wakili, S. Clauss, V. Schmidt, M. Ulbrich, A. Hahnefeld, F. Schüssler, J. Siebermair, S. Kääb, and H. L. Estner, "Impact of real-time contact force and impedance measurement in pulmonary vein isolation procedures for treatment of atrial fibrillation," *Clinical Research in Cardiology*, vol. 103, no. 2, pp. 97–106, 2014.

[14] J. G. Andrade, G. Monir, S. J. Pollak, P. Khairy, M. Dubuc, D. Roy, M. Talajic, M. Deyell, L. Rivard, B. Thibault *et al.*, "Pulmonary vein isolation using contact force ablation: the effect on dormant conduction and long-term freedom from recurrent atrial fibrillationa prospective study," *Heart Rhythm*, vol. 11, no. 11, pp. 1919–1924, 2014.

[15] A. Thiagalingam, A. DAVILA, L. Foley, J. L. Guerrero, H. Lambert, G. Leo, J. N. Ruskin, and V. Y. Reddy, "Importance of catheter contact force during irrigated radiofrequency ablation: evaluation in a porcine ex vivo model using a force-sensing catheter," *Journal of cardiovascular electrophysiology*, vol. 21, no. 7, pp. 806–811, 2010.

[16] C. Sohns, R. Karim, J. Harrison, A. Arujuna, N. Linton, R. Sennett, H. Lambert, G. Leo, S. Williams, R. Razavi *et al.*, "Quantitative magnetic resonance imaging analysis of the relationship between contact force and left atrial scar formation after catheter ablation of atrial fibrillation," *Journal of cardiovascular electrophysiology*, vol. 25, no. 2, pp. 138–145, 2014.

[17] W. Saliba, V. Y. Reddy, O. Wazni, J. E. Cummings, J. D. Burkhardt, M. Haissaguerre, J. Kautzner, P. Peichl, P. Neuzil, V. Schibgilla *et al.*, "Atrial fibrillation ablation using a robotic catheter remote control system: initial human experience and long-term follow-up results," *Journal of the American College of Cardiology*, vol. 51, no. 25, pp. 2407–2411, 2008.

[18] L. Di Biase, Y. Wang, R. Horton, G. J. Gallinghouse, P. Mohanty, J. Sanchez, D. Patel, M. Dare, R. Canby, L. D. Price *et al.*, "Ablation of atrial fibrillation utilizing robotic catheter navigation in comparison to manual navigation and ablation: Single-center experience," *Journal of cardiovascular electrophysiology*, vol. 20, no. 12, pp. 1328–1335, 2009.

[19] J. Jayender, M. Azizian, and R. V. Patel, "Autonomous image-guided robot-assisted active catheter insertion," *IEEE Transactions on Robotics*, vol. 24, no. 4, pp. 858–871, 2008.

[20] S. G. Yuen, M. C. Yip, N. V. Vasilyev, D. P. Perrin, J. Pedro, and R. D. Howe, "Robotic force stabilization for beating heart intracardiac surgery," in *International Conference on Medical Image Computing and Computer-Assisted Intervention*. Springer, 2009, pp. 26–33.

[21] S. B. Kesner and R. D. Howe, "Robotic catheter cardiac ablation combining ultrasound guidance and force control," *The International Journal of Robotics Research*, vol. 33, no. 4, pp. 631–644, 2014.

[22] M. C. Yip, J. A. Sganga, and D. B. Camarillo, "Autonomous control of continuum robot manipulators for complex cardiac ablation tasks," *Journal of Medical Robotics Research*, vol. 2, no. 01, p. 1750002, 2017.

[23] T. Greigarn, R. Jackson, T. Liu, and M. C. Çavuşoğlu, "Experimental validation of the pseudo-rigid-body model of the MRI-actuated catheter," in *Robotics and*

Automation (ICRA), 2017 IEEE International Conference on. IEEE, 2017, pp. 3600–3605.

[24] T. Greigarn and M. C. Çavuşoğlu, "Pseudo-rigid-body model and kinematic analysis of MRI-actuated catheters," in *Robotics and Automation (ICRA), 2015 IEEE International Conference on*. IEEE, 2015, pp. 2236–2243.

[25] M. Khoshnam and R. V. Patel, "A pseudo-rigid-body 3r model for a steerable ablation catheter," in *2013 IEEE International Conference on Robotics and Automation*. IEEE, 2013, pp. 4427–4432.

[26] H.-J. Su, "A pseudorigid-body 3r model for determining large deflection of cantilever beams subject to tip loads," *Journal of Mechanisms and Robotics*, vol. 1, no. 2, p. 021008, 2009.

[27] T. Greigarn, N. L. Poirot, X. Xu, and M. C. Cavusoglu, "Jacobian-based task-space motion planning for MRI-actuated continuum robots," *IEEE Robotics and Automation Letters*, 2018.

[28] T. Greigarn and M. C. Çavuşoğlu, "Task-space motion planning of MRI-actuated catheters for catheter ablation of atrial fibrillation," in *Intelligent Robots and Systems (IROS 2014), 2014 IEEE/RSJ International Conference on*. IEEE, 2014, pp. 3476–3482.

[29] R. M. Murray, *A mathematical introduction to robotic manipulation*. CRC press, 2017.

[30] T. Greigarn, "Kinematics, planning, and perception for magnetically-actuated MRI-guided continuum robots," Ph.D. dissertation, Case Western Reserve University, 2018.

[31] R. Ginhoux, J. A. Gangloff, M. F. de Mathelin, L. Soler, M. M. A. Sanchez, and J. Marescaux, "Active filtering of physiological motion in robotized surgery using predictive control," *IEEE Transactions on Robotics*, vol. 21, no. 1, pp. 67–79, February 2005.

[32] T. Ortmaier, M. Groger, D. H. Boehm, V. Falk, and G. Hirzinger, "Motion estimation in beating heart surgery," *IEEE Transactions on Biomedical Engineering*, vol. 52, pp. 1729–1740, October 2005.

[33] O. Bebek and M. C. Çavuşoğlu, "Intelligent control algorithms for robotic-assisted beating heart surgery," *IEEE Transactions on Robotics*, vol. 23, no. 3, pp. 468–480, 2007.

[34] S. G. Yuen, D. T. Kettler, P. M. Nonotny, R. D. Plowes, and R. D. Howe, "Robotic motion compensation for beating heart intracardiac surgery," *International Journal of Robotics Research*, vol. 28, no. 10, pp. 1355–1372, October 2009.

[35] E. E. Tuna, T. J. Franke, O. Bebek, A. Shiose, K. Fukamachi, and M. C. Cavusoglu, "Heart motion prediction based on adaptive estimation algorithms for robotic-assisted beating heart surgery," *IEEE Transactions on Robotics*, vol. 29, no. 1, pp. 261–276, 2012.

[36] E. E. Tuna, K. J. H., T. Liu, O. Bebek, K. Fukamachi, and M. C. Çavuşoğlu, "Towards active tracking of beating heart motion in the presence of arrhythmia for robotic assisted beating heart surgery," *PLoS One*, vol. 9, no. 7, p. e102877, 2014.

[37] M. C. Çavuşoğlu, J. Rotella, W. S. Newman, S. Choi, J. Ustin, and S. S. Sastry, "Control algorithms for active relative motion cancelling for robotic assisted off-pump coronary artery bypass graft surgery," in *Proceedings of the 12th International Conference on Advanced Robotics (ICAR 2005)*, July 2005, pp. 431–438.

[38] T. Greigarn, T. Liu, and M. C. Çavuşoğlu, "Parameter optimization of pseudo-rigid-body models of MRI-actuated catheters," in *Engineering in Medicine and Biology Society (EMBC), 2016 IEEE 38th Annual International Conference of the*. IEEE, 2016, pp. 5112–5115.

[39] E. E. Tuna, T. Liu, R. Jackson, N. L. Poirot, M. Russell, and M. C. Çavuşoğlu, "Analysis of dynamic response of an MRI-guided magnetically-actuated steerable catheter system," in *Proceedings of the IEEE/RSJ International Conference on Intelligent Robots and Systems (IROS 2018)*, 2018, Conference Proceedings, pp. 4927–4934.